NASA TECHNICAL MEMORANDUM

NASA TM X-2920

NASA TM X-2920

VIBRATION BEHAVIOR OF FUEL-ELEMENT VIBRATION SUPPRESSORS FOR THE ADVANCED POWER REACTOR

by Donald W. Adams and Ivan B. Fiero

Lewis Research Center

Cleveland, Ohio 44135

NATIONAL AERONAUTICS AND SPACE ADMINISTRATION • WASHINGTON, D. C. • NOVEMBER 1973

1. Report No.	2. Government Accession No.	3. Recipient's Catalog No.
NASA TM X-2920		

4. Title and Subtitle	5. Report Date
VIBRATION BEHAVIOR OF FUEL-ELEMENT VIBRATION SUPPRESSORS FOR THE ADVANCED POWER REACTOR	November 1973
	6. Performing Organization Code
7. Author(s)	8. Performing Organization Report No.
Donald W. Adams and Ivan B. Fiero	E-6816
	10. Work Unit No.
9. Performing Organization Name and Address	503-25
Lewis Research Center National Aeronautics and Space Administration Cleveland, Ohio 44135	11. Contract or Grant No.
	13. Type of Report and Period Covered
12. Sponsoring Agency Name and Address	Technical Memorandum
National Aeronautics and Space Administration Washington, D. C. 20546	14. Sponsoring Agency Code

15. Supplementary Notes

16. Abstract

Preliminary shock and vibration tests were performed on vibration suppressors for the advanced power reactor for space application. These suppressors position the fuel pellets in a pin type fuel element. The test determined the effect of varying axial clearance on the behavior of the suppressors when subjected to shock and vibratory loading. The full-size suppressor was tested in a mockup model of fuel and clad which required scaling of test conditions. The test data were correlated with theoretical predictions for suppressor failure. Good agreement was obtained. The maximum difference with damping neglected was about 30 percent. Neglecting damping would result in a conservative design.

17. Key Words (Suggested by Author(s))	18. Distribution Statement
Fuel element vibration Vibration suppression Space power reactors Environmental testing, vibration	Unclassified - unlimited

19. Security Classif. (of this report)	20. Security Classif. (of this page)	21. No. of Pages	22. Price*
Unclassified	Unclassified	30	Domestic, $3.00 Foreign, $5.50

* For sale by the National Technical Information Service, Springfield, Virginia 22151

VIBRATION BEHAVIOR OF FUEL-ELEMENT VIBRATION SUPPRESSORS FOR THE ADVANCED POWER REACTOR

by Donald W. Adams and Ivan B. Fiero
Lewis Research Center

SUMMARY

Preliminary shock and vibration tests and analysis were performed on collar-button (spool) shaped vibration suppressors. These suppressors position axially and accommodate the thermal expansion and axial swelling of the fuel pellets in the fuel element for a space power nuclear reactor, the advanced power reactor. The suppressors also provide a collection space for fission gases.

The purpose of the test program and the analysis was to determine the structural capabilities of the suppressors when they are exposed to the shock and vibration loading that a nuclear reactor may encounter during launch into space.

The tests included full-size suppressors, but the fuel pellets were simulated. Suppressors were tested with a fixed diametral clearance but with a variety of axial clearances, column sizes, and materials. These were destructive tests carried to failure, from which a final load capability could be determined. This experimental failure load was compared to the predicted failure load in an effort to evaluate the theory.

The first tests were run with specimens of T-111 material and of a geometry that contained a dished end (Belleville) spring. The first test was with launch vibration specifications; two more tests followed with modified vibration specifications. The specimens failed because the dished end acted as an effective gap which increased the shock loads in the column of the suppressor. The design of the suppressor was subsequently modified to eliminate this problem.

Further tests were run on specimens of other materials and with geometries that did not have dished ends. These tests were run with a variety of axial gaps and at a constant frequency of 200 hertz.

The data that resulted from these controlled tests agree very well with theoretical predictions of failure loads. If damping in the system were neglected, the agreement would still be within approximately 30 percent for the worst case tested. Neglecting the damping would also result in a conservative design (since the damping acts to reduce the load). Because of the uncertainty in the damping and because of the scaling of test conditions, it may be desirable in a later test phase to proof test the vibration suppressor in a full-scale test at launch vibration specifications to ensure the feasibility of the design.

INTRODUCTION

Vibration suppressors are being considered as retainer devices for the fuel pellet stack within the fuel pins of the advanced power reactor (APR). The APR is a compact fast reactor concept being investigated for potential space power application. It is described in detail in reference 1.

A fuel element with typical vibration suppressors is shown in figure 1. The purpose of the axial space beyond the fuel stack shown in the figure is twofold. First, it acts as a thermal expansion and fuel swelling sink. Second, it acts as a fission gas collection space. Radial voids also exist for these same purposes. Axial spacers are required to position the fuel. These spacers must accommodate axial fuel growth but inhibit motions that could lead to failures under launch or transport vibration conditions. The column structure of the vibration suppressors shown is intended to serve this function. Final axial gaps between fuel, vibration suppressor, and end cap may also occur at assembly, mainly because of unknown amounts of weld shrinkage. Fuel pellet vibration tests, reported in reference 2, indicated that the maximum axial clearance permissible for the presently available methods of fabricating fuel pellets was 0.025 millimeter (0.001 in.). Greater gaps resulted in fuel-pellet disintegration during vibration testing. Consequently, the vibration suppressor is a critical member of the fuel-pin design in that its potential failure load with various axial gaps must be accurately known. Since it must collapse under the loading from swelling fuel, it should be only strong enough to withstand vibratory loads during launch.

Both a theoretical and an experimental approach were undertaken to determine the effect of axial clearance on the vibration suppressor. The theoretical approach was to achieve a time-dependent solution for the compression of the column. The experimental approach consisted of placing the suppressors in a container with varying degrees of axial clearance between the suppressor, simulated pellets, and container. The test package was then vibrated and shock loaded over ranges induced by launch conditions. Following these tests visual examination was performed to observe any structural damage. Early failures of the test specimens required a modification of the design concept and the test procedure as well as adding static buckling tests to understand better what was taking place.

THEORY

The dynamic model of the fuel pin consists of a single vibration suppressor, the fuel mass, and the container. All components of the fuel pin, shown in figure 1, are large compared with the diameter of the column of the vibration suppressor. Therefore, all

components other than the column will be treated as rigid masses. The column will be treated as an equivalent spring, and an equivalent damper will be added. This system is shown schematically in figure 2. The impact velocity of the mass will be treated as a parameter determined from another model. A detailed time history would present uncertainty in the impact velocity because of uncertainties resulting from damping as the fuel moves across the gap. The damping in the system comes from material deformation in the column, scraping and sliding of components, and aerodynamic drag. The damping will also be treated as a parameter.

The effective spring constant k is determined from classical theory as

$$k = \frac{EA_c}{l} \tag{1}$$

where E is the modulus of elasticity and A_c and l are the column cross-sectional area and length, respectively.

First, the impact velocity must be determined. The sequence of events leading up to impact is shown schematically in figure 3. It was assumed that a buildup of velocity from one cycle to the next would not occur because of the friction and aerodynamic drag on the fuel after it bounces off the spring. It is assumed that the entire system, which is rigidly fastened to the shake table, accelerates up to the maximum velocity, as shown in figure 3(a). At this point the fuel mass continues at maximum velocity across the gap Δx. The fixture continues to follow the table acceleration, as shown in figure 3(b). Consequently, at impact there is a net impact velocity of the fuel mass on the spring.

The maximum velocity of the fuel or the fixture is

$$V_{max} = y\omega_1 \tag{2}$$

$$Y = \frac{g}{\omega_1^2} \tag{3}$$

After reaching maximum velocity the fixture decelerates so that the fixture velocity is

$$V_1 = V_{max} \cos \omega_{1t} \tag{4}$$

The net velocity at impact is $V_{max} - V_1$. After maximum velocity is attained, the displacements of the fuel mass and fixture are

$$x_f = \int_0^{t_0} V_{max}\, dt \tag{5}$$

$$x_t = \int_0^{t_0} V_{max}\, dt \tag{6}$$

Impact occurs when the gap Δx between the fuel and suppressor closes:

$$x_f - x_t = \Delta x \tag{7}$$

$$V_{max} \int_0^{t_0} (1 - \cos \omega_1 t)dt = \Delta x \tag{8}$$

$$V_{max}\left(\frac{\omega_1 t_0 - \sin \omega_1 t_0}{w_1}\right) = \Delta x \tag{9}$$

Substituting the value of V_{max} from equation (3) and rearranging yield

$$\alpha - \sin(\alpha) = \frac{\Delta x}{Y} \tag{10}$$

where

$$\alpha = \omega_1 t_0$$

This is a very smooth function and can easily be solved for α by using an iterative technique. The limitation should be imposed here that the angle α cannot exceed π. This simply means that the table moves through more than one-half cycle to come into contact. If this should occur, it would be a better assumption that the velocity at impact is a maximum of twice the table velocity. This assumption is also in line with the assumed random nature of the movement across the gap. For small gaps, however, this need not be considered unless the acceleration level of the input function is high (small Y).

Further behavior after impact can be described by a simple spring mass system, as shown in figure 3(c). This model is valid only while the spring (vibration suppressor) is

in compression. The spring never experiences tensile forces because it is not attached to the mass or the fixture. If the mass of the fuel is large compared with the mass of the column, the effect of wave motion along the column can be neglected and the force is assumed to be transmitted instantaneously through the column (ref. 3). It will be assumed that the gravitational force is in the positive direction (this was the case for the test program) and that the zero-displacement position corresponds to the zero-compression position. The equilibrium equation for the system is

$$m\ddot{x} + cx + kx - mg - kx_1 - c\dot{x}_1 = 0 \tag{11}$$

or

$$\ddot{x} + \frac{c}{m}\dot{x} + \frac{k}{m}x = g + \frac{k}{m}x_1 + \frac{c}{m}\dot{x}_1 \tag{12}$$

If we let

$$\omega^2 = \frac{k}{m} \tag{13a}$$

$$c = \xi c_c \tag{13b}$$

and

$$c_c = 2m\omega \tag{13c}$$

the equilibrium equation becomes

$$\ddot{x} + 2\omega\xi\dot{x} + \omega^2 x = g + \omega^2 x_1 + 2\omega\xi\dot{x}_1 \tag{14}$$

The relative position of the fixture after impact can be expressed as

$$x_1 = Y \sin(\omega_1 t + \alpha) - Y \sin(\alpha)$$

Expanding the first term and substituting into equation (14) yield

$$\ddot{x} + 2\omega\xi\dot{x} + \omega^2 x = g + (Y\omega^2 \sin\alpha + 2Y\omega\omega_1\xi \cos\alpha)\cos\omega_1 t$$

$$+ (Y\omega^2 \cos\alpha - 2Y\omega\omega_1\xi \sin\alpha)\sin\omega_1 t - Y\omega^2 \sin\alpha \qquad (15)$$

If the table frequency is different from the natural frequency, the solution is

$$x = Ae^{-\xi\omega t} \sin \sqrt{1-\xi^2}\,\omega t + Be^{-\xi\omega t} \cos \sqrt{1-\xi^2}\,\omega t$$

$$+ C_1(g - x\omega^2 \sin\alpha) + C_2 \cos\omega_1 t + C_3 \sin\omega_1 t \qquad (16)$$

Applying the boundary conditions that

$$\left.\begin{aligned} x &= 0 \quad \text{at} \quad t = 0 \\ \dot{x} &= V_{max} \quad \text{at} \quad t = 0 \end{aligned}\right\} \qquad (17)$$

and substituting the solution into the differential equation result in

$$A = -\frac{1}{\sqrt{1-\xi^2}}\left\{\left[C_1(g - Y\omega^2 \sin\alpha) + C_2\right]\xi + C_3\gamma - \frac{V_{max}}{\omega}\right\} \qquad (18a)$$

$$B = -C_1(g - Y\omega^2 \sin\alpha) - C_2 \qquad (18b)$$

$$C_1 = \frac{1}{\omega^2} \qquad (18c)$$

$$C_2 = \frac{Y\left[(1 - \gamma^2 + 4\gamma^2\xi^2)\sin\alpha - 2\gamma^3\xi \cos\alpha\right]}{\left(1 - r^2\right)^2 + (2r\xi)^2} \qquad (18d)$$

$$C_2 = \frac{Y\left[2\gamma^3\xi \sin\alpha + (1 - \gamma^2 + 4\gamma^2\xi^2)\cos\alpha\right]}{\left(1 - \gamma^2\right)^2 + (2\gamma\xi)^2} \qquad (18e)$$

where

$$\gamma = \frac{\omega_1}{\omega} \tag{19}$$

An expression for the compression of the column is, therefore, the difference between x and x_1, or

$$\delta = x - x_1 \tag{20}$$

The strain in the column is

$$\epsilon = \frac{\delta}{l} \tag{21}$$

and the stress is

$$\sigma = E\epsilon \tag{22}$$

Combining equations gives

$$\sigma = \frac{E}{l}(x - x_1) \tag{23}$$

An equivalent static stress load for vibrating systems is often defined as

$$\sigma_s = \frac{m\omega_1^2 Y}{A_c} \tag{24}$$

where the terms $\omega_1^2 Y$ represents the peak acceleration. A load factor can then be defined as

$$L_f = \frac{\sigma}{\sigma_s} = \frac{EA_c}{ml\omega_1^2 Y}(x - x_1) \tag{25}$$

and the shock factor, called the maximum load factor in this report, can be defined as

$$S_f = \max(L_f) \tag{26}$$

If the table frequency is identical to the natural frequency and the damping is zero, the solution of the differential equation is

$$x = A \cos \omega_1 t + B \sin \omega_1 t + C_1\left(g - Y\omega_1^2 \sin \alpha\right) + C_2 t \cos \omega_1 t + C_3 t \sin \omega_1 t \qquad (27)$$

where

$$A = -C_1\left(g - Y\omega_1^2 \sin \alpha\right) \qquad (28a)$$

$$B = \frac{V_{max} - C_2}{\omega_1} \qquad (28b)$$

$$C_1 = \frac{1}{\omega_1^2} \qquad (28c)$$

$$C_2 = -\frac{1}{2}\omega_1 Y \cos \alpha \qquad (28d)$$

$$C_3 = \frac{1}{2}\omega_1 Y \sin \alpha \qquad (28e)$$

Equation (27) describes the behavior during the transient period after impact.

TEST PROGRAM

Test Consideration and Procedure

Initially the test conditions for the suppressors were to follow the shock and vibration loads as specified in the fuel pellet tests of reference 2. These loads were for the payload area of the Saturn V launch vehicle (ref. 4) but were modified to include the more stringent loads of the SNAP 8 environmental specification dated March 31, 1967 (ref. 5). Sinusoidal and random vibration test conditions are shown in figures 4 and 5.

The suppressors were designed so that they would not fail in buckling at twice the expected equivalent static load. Buckling equations with the worst possible end conditions, one fixed end and one free end, were used for this purpose. However, failure of

the first T-111 specimen at well below the design load necessitated a change in test procedure and test conditions. The modified procedure and conditions consisted of vibrating the specimen at a constant frequency of 200 hertz and gradually increasing the acceleration loading in steps. Thus, the test procedure became one of exploring what was physically happening, rather than proof testing following the prescribed launch loads. The frequency of 200 hertz was chosen, as this frequency at the prescribed acceleration load for launch, gives the largest fixture amplitude.

This procedure allows one to determine at what load the specimens failed. This is difficult to do when following the scanning procedure specified for these tests in references 4 and 5, because the output instrumentation could not easily detect failure at a specific frequency. The maximum load considered was 70.2 g's, as shown in figure 4. This test value was higher than the specification value because the total weight of the T-111 spacer (simulating the pellets) above the suppressor was less than the actual total weight of the fuel pellets in a fuel assembly. This difference was compensated for by increasing the g-value proportionally. Included in the g-value was a 6-g acceleration load which was added to the specification value because of additional launch acceleration in the axial direction only.

The early failure of the T-111 suppressor also brought about the decision to switch from T-111 specimens to stainless-steel (17-4PH) specimens. This change was made because stainless steel was considerably cheaper, readily available, and easier to machine, and the modulus of elasticity, a parameter affecting buckling, is nearly identical to that of T-111. Also for test purposes the Belleville type flange on the suppressor was eliminated as it was another source of uncertainty.

Later tests were also conducted on specimens made of ingot iron, which has a modulus of elasticity similar to those of T-111 and stainless steel; however, the yield point for ingot iron is much less than those of T-111 or stainless steel. This switch in materials was decided upon since static column buckling tests on the stainless-steel specimens showed the failure mode of the structure as yielding rather than true buckling. Deformations in the failed specimen were more suggestive of built-in ends. The yield load is less than that for true buckling for such materials and end conditions. With this type of failure, the load capacity of the stainless-steel specimens was high compared to the capacity of the shake table. Ingot iron, therefore, with its lower yield strength was used. The ingot iron specimen would fail within the testing range of the shaker, and the shaft diameter could be reasonably sized for easy machining.

Test Specimen

The three initial specimens, of the basic conceptual design, were manufactured from T-111 with the geometry shown in figure 6(a). The dished flange shown behaved

similar to a Belleville spring and was intended to provide zero clearance betwen the end cap and the fuel pellets by absorbing the end-cap weld shrinkage while restraining the pellets when subjected to launch-induced vibratory loads.

The second series of specimens was made of stainless steel (17-4PH) with the geometry shown in figure 6(b) and with the shaft dimensions given in table I, tests 6 and 8 to 12, and in table II. The dished-head concept was discarded since the pellet test results given in reference 2 limited axial clearances to 0.025 millimeter (0.001 in.) or less and early failures of the suppressor indicated that the dished head resulted in greater than permissable motion of the suppressor. Two of the stainless-steel specimens (8 and 9) were instrumented with strain gages.

The third series of specimens was made of ingot iron. The geometry is shown in figure 6(b) and the shaft dimensions are given in table III.

Test Fixture

A sketch of the test fixture is shown in figure 7 and described in detail in reference 2. This fixture had a bore of 1.58 centimeters (0.632 in.) which gave a diametral clearance of less than 0.025 millimeter (0.001 in.). The suppressor was located at one end with a T-111 spacer (simulated fuel) in the remaining space. The axial clearance was set by the T-111 spacer and the end caps with the metal spacing shims. The fixture had been checked for natural frequencies in the operating range of 20 to 2000 hertz (ref. 4), and none were observed. During the axial vibration tests the fixture was vibrated in the vertical position as shown in figure 8 with the vibration suppressor mounted at the bottom. In addition to positioning of the suppressor, the T-111 spacer provides a weight which simulates the fuel load (as noted in the previous section). The test g-loads required to produce the actual loads which exist on the lower suppressor of a complete fuel element were determined as follows:

$$g_{test} = (g_{specification} + 6)\left(\frac{\text{total fuel weight in a complete fuel element}}{\text{T-111 weight}}\right)$$

Apparatus and Instrumentation

The apparatus used for the vibration tests was a shaker with a capacity of 26 700 newtons (6000 lb force). It is described in reference 2.

For the shock tests a drop tester was used; this tester is also described in reference 2.

The static buckling tests were run on a tensile tester with a maximum load capacity of 44 800 newtons (10 000 lb). These tests were run at about 2240 newtons (500 lb). The load was applied to the specimen, and the strain was read directly on the strip chart of the tester. Later (specimen 5, table II) dial indicators were used to detect shaft bowing. Strain gages were also installed on specimen 9. The strain gages were mounted 90^{o} apart so that regardless of how the shaft buckled a reading or combination of readings was obtained. The strains were read on a separate x-y-y plotter. The stress readings were obtained by a separate load cell mounted in series with the specimen.

RESULTS AND DISCUSSION

The results of the tests are summarized in tables I to III. Table I presents the data for the axial dynamic tests for the T-111 and the stainless-steel suppressors. Table II presents the data for the axial static tests for the stainless-steel specimens, while table III presents the data for the axial dynamic tests for the ingot iron specimens.

T-111 Specimens

The first three tests (1 to 3) are for the specimens made of T-111 material and to the basic conceptual design (fig. 6(a)). The first suppressor (1) survived the shock tests, and the random and sinusoidal diametral vibration tests as required in reference 2. However, it failed during the initial axial sinusoidal vibration frequency sweep of 70.5 g's (fig. 4). Figure 9 shows the failed suppressor. The end clearance was set at less than 0.025 millimeter (0.001 in.). However, the movement may have been greater because of the 0.076-millimeter- (0.003-in.-) deep dished end flange (Belleville spring concept). The exact loading at failure was impossible to determine because the frequency range is covered by a sweep type mode of operation, as shown in figure 4. This premature failure, plus the inability to determine the failure load, resulted in a decision to change the test procedure. The new procedure consisted of imposing a constant frequency (200 Hz) with a graduated increase in g-loading. It was also decided to concentrate on the axial vibration tests, since the successful diametral tests on the first specimen were sufficient. For all of the remaining tests of T-111, a diametral clearance of less than 0.025 millimeter (0.001 in.) existed.

The loads on specimens 2 and 3 in table I were increased from 5 to approximately 50 g's at 10-minute time durations for each g-load. Premature failure again occurred. It was apparent that more extensive testing would be necessary to resolve this failure problem.

Stainless-Steel Specimens

Rather than continue testing with T-111 specimens, new specimens made of 17-4PH stainless steel were used. This material was chosen because it is cheaper and because its modulus of elasticity is about the same as that of T-111. Therefore, its buckling behavior should be about the same. The modulus of elasticity is important in modeling buckling, and at this point the mode of failure was unknown. The high strength of stainless steel also was intended to help remove this parameter as an unknown in the effort to resolve the failure problem.

The specimens had two thick flanges to eliminate the spring effect of the dished flange and to set the required end clearance more accurately at 0.025 and 0.076 millimeter (0.001 and 0.003 in.) (see fig. 6(b)). The dished flange was a compromise between the requirements that it deflect up to 0.076 millimeter (0.003 in.) without failure of the column (this spring load must be added to launch loads for the column design) and that it be sufficiently strong to be meaningful. It appeared that during these lengthy hold times of 10 minutes the dished flange tended to flatten permanently and thereby increased the effective gap size.

Static Buckling Tests

The first tests with the stainless-steel specimens were static buckling tests. The purposes of these tests were to (1) check and compare results with original buckling calculations, (2) determine if the suppressors failed as a true column under buckling conditions, and (3) determine the actual yield stress of the suppressor material used.

Four specimens were tested. The results of these tests are presented in table II (specimens 4, 5, 7, and 9). The calculated critical buckling loads for columns of different diameters and different possible end conditions are shown as indicated in figure 10. Superimposed on the plot are the yield stress curves for T-111, stainless steel, and ingot iron. The upper stainless-steel point (specimen 9, table II) is the static buckling test data. The remarks in table II indicate why other points were not included. The resulting conclusion was that the specimens did not fail in buckling but rather that they failed in yield at a predictable load for that mode. This data point falls nearly on the stainless-steel yield curve. If it were to have failed in buckling under the end conditions observed, the buckling load would be far above the actual failure load.

The results also showed that yield loads were approximately 10 percent higher than the published values of tensile yield for 17-4PH condition H1150 stainless steel (ref. 6).

Dynamic Tests

Concurrently with the static tests, axial vibration tests were run with stainless-steel specimens (table I, specimens 6 and 8 to 12). The first of these vibration tests (6 and 8 to 10) were run with specimens having 1.5-millimeter- (0.060-in.-) diameter shafts. They were vibrated by using the modified procedure (200 Hz with loads from 5 to 100 g's for 1 min at each g-load). One hundred g's is the shaker limit. The axial clearance was set at less than 0.025 millimeter (0.001 in.) as well as 0.076 millimeter (0.003 in.). There were no failures for these 1-minute runs. Specimen 8 was further tested at a 100-g load; it failed after 5 minutes. This is shown as the lower stainless-steel dynamic failure point in figure 10. The last two stainless-steel specimens (11 and 12) had a reduced shaft diameter of 1.016 millimeter (0.040 in.). The small diameter was an attempt to ensure specimen failure as well as to have failure points with various size shaft diameters. The first of these two specimens (11) was tested with an axial clearance less than 0.025 millimeter (0.001 in.) and at 200 hertz. At a load of 90 g's the table "fired" and stopped, and the specimen collapsed. This firing is an abrupt halt of the table when the overload switch cuts off the table power. The sudden halt can cause very high, unpredictable g-loads. Thus, it was not certain whether the specimen failed because of firing the table or vice versa. The second 1.016-millimeter-(0.040-in.-) diameter specimen (12) was tested but with a 0.076- to 0.1-millimeter (0.003- to 0.004-in.) axial clearance. Once more the table fired, and the specimen failed, only this time at a load of 70 g's. This firing was caused by an accidental power shutdown.

The static test results indicated the stainless-steel specimens may have been too strong to fail at this given shaker limitation. Trying to cause failure by making the shaft less than 1.016 millimeters (0.040 in.) was a possibility but presented machining problems.

Ingot Iron

It was decided to make five specimens of low-yield-strength ingot iron and conduct vibration tests. The specimens had 1.5-millimeter- (0.060-in.-) diameter shafts (the geometry in fig. 6(b)).

One of the purposed of these tests was to have a range of specimens with different apparent failure stresses in an effort to establish a shock factor (ratio of static yield stress to apparent dynamic yield stress or failure stress) which might correlate the results. The other purpose was to verify buckling or yield failure. A tensile test was also made on the material to obtain the actual yield point, which was found to be 19 400 newtons per square centimeter (28 150 psi).

These specimens were all vibrated with a diametral clearance of less than 0.025 millimeter (0.001 in.) and axial clearances of 0.025, 0.051, and 0.076 millimeter (0.001, 0.002, and 0.003 in.). All were tested at 200 hertz with gradually increasing g-loads (held for 1 min). All specimens failed at values fairly close to those predicted from theory. A typical failed specimen is shown in figure 11.

The results of the tests are given in table III.

Test specimens 1 and 4 were run with less than 0.025-millimeter (0.001-in.) axial clearance and failure occurred at loads of 40 and 39 g's respectively. Test specimen 3 was run with 0.05-millimeter (0.002-in.) axial clearance and failed at a load of 30 g's. Test specimens 2 and 5 were run with 0.076-millimeter (0.003-in.) axial clearance and both failed at a load of 23 g's.

Correlation and Use of Data

The failure data for the ingot iron specimens can be predicted very well with the theory outlined previously. A plot of equation (25) appears in figure 12 for some specific conditions that correspond to geometry and load level at failure. The maximum compression of the column is sensitive to the fraction of critical damping in the system. Since this is somewhat of an unknown, several values are shown. Characteristic of these curves is the fact that the load factor returns to zero at some point in time (at which the solution is no longer valid). The failure points have also been shown in the figure. It is apparent from this figure that the damping increases with gap size. This would be reasonable because the larger gap (over the range considered in the figure) results in larger impact velocity. All the sources of damping increase with impact velocity. It also can be concluded that a design based on zero damping would be conservative. Such a design would be, at most, 10 percent conservative with a 0.025-millimeter (0.001-in.) gap and approximately 30 percent conservative with a 0.076-millimeter (0.003-in.) gap.

Since curves such as shown in figure 12 are dependent on knowing the failure load, they are not generally useful in actually predicting failure. Consequently, only the maximum load factor (eq. (26)) need be considered. A plot of the shock factor (maximum load factor) is shown in figure 13. The additional parameter here is the input load (g-level). In order to predict failure load the yield curve is required. This is obtained by dividing the yield stress by the equivalent static stress given by equation (24). The resulting ratio is the shock factor. In other words, when the shock factor multiplied by the equivalent static stress equals the yield stress, failure will occur. The point where the shock factor from the yield criteria intersects the curve from equation (26) is the failure point. The load level at which failure would occur can then be determined. Failure points for the test data are shown in figure 13. Here, as indicated for figure 12, the

value of the damping factor plays an important role in determining the exact failure point. It should be noted that the values indicated by the curves in figure 13 are slightly different from those in figure 12. This difference is due to an approximate technique used to find the maximum value of the function given in equation (25).

The data for the T-111 specimens cannot be correlated as easily as those for the ingot iron specimens. The apparent premature failure was due primarily to the spring effect of the dished end and to its flattening during the testing. As a result, the end design of the suppressor was changed to that shown in figure 14. The suppressor can be screwed into the end cap, the end cap welded to the clad, and then the supressor screwed back into the fuel pin until it is tight. The seal weld can then be annealed by utilizing chill blocks on the end cap portion. The theory developed and proven for the ingot iron suppressors can then be used to design the T-111 suppressor.

CONCLUSIONS

The results of a study of the vibration behavior of fuel-element vibration suppressors for the advanced power reactor have led to the following conclusions:

1. The end condition on the suppressor appears to be somewhere between those of a hinged and a fixed end. As a result the column fails by simple yielding. Buckling through instability requires a higher load than yielding.

2. The vibration suppressor needed redesign to eliminate the unknown effect of the dished flange. It appeared to act as an equivalent larger gap. The redesigned suppressor allows final adjustment to eliminate the gap.

3. Theoretical predictions can be adequately used to determine loads in the column. Theoretically predicted values of the loads agreed to within 10 to 30 percent of experimentally measured loads.

4. When damping is neglected, the theoretical predictions are always conservative.

5. Because of uncertainties in determining damping, it may be desirable to further proof test the vibration suppressor in a full-scale test. This test should use fuel pellets and be run with launch and shock load specifications.

Lewis Research Center,
National Aeronautics and Space Administration,
Cleveland, Ohio, July 27, 1973,
503-25.

APPENDIX - SYMBOLS

A	arbitrary constant
A_c	column cross-sectional area, m^2
B	arbitrary constant
C_1, C_2, C_3	arbitrary constants
c	coefficient of damping, N/(m/sec)
c_c	critical damping coefficient, N/(m/sec)
E	modulus of elasticity, N/m^2
g	gravitational acceleration, 9.80 m/sec^2
k	spring constant, N/m
L_f	load factor
l	column length, m
m	mass, kg
S_f	shock factor, Y_s/Y_d
t	time, sec
v	velocity, m/sec
x	displacement of mass, m
x_1	displacement of table, m
Δx	gap size, m
Y	table amplitude, m
α	phase angle
γ	frequency ratio
δ	compression of column, m
ϵ	strain in column, m/m
ξ	damping factor
σ	stress in column, N/m^2
σ_s	equivalent static stress, N/m^2
ω	natural freauency of column, sec^{-1}
ω_1	forcing frequency of table, sec^{-1}

Subscripts:

c	column
d	dynamic
f	fuel
max	maximum
s	static
t	table
0	initial value

REFERENCES

1. Krasner, Morton H.; Davison, Harry W.; and Diaguila, Anthony J.: Conceptual Design of a Compact Fast Reactor for Space Power. NASA TM X-67859, 1971.

2. Adams, Donald W.: Shock and Vibration Tests of Uranium Mononitride Fuel Pellets for a Space Power Nuclear Reactor. NASA TM X-2493, 1972.

3. Timoshenko, Stephen: Vibration Problems in Engineering. Third ed., D. Van Nostrand Co., Inc., 1955.

4. Schulte, L. O.: Saturn V Payload Planner's Guide. Rep. SM-47274, Douglas Aircraft Co., Inc., Nov. 1965.

5. Anon.: Environmental Specification for SNAP 8 Electrical Generating System. Spec. No. 417-2, NASA Lewis Research Center, Mar. 31, 1967.

6. Ludwigson, D. C.; and Hall, A. M.: The Physical Metallurgy of Precipitation-Hardenable Stainless Steels. DMIC Rep. 111, Batelle Memorial Inst. (AD-214001), Apr. 20, 1959.

7. Sheffler, K. D.; Sawyer, J. C.; and Steigerwald, E. A.: Creep Behavior of Refractory Alloys in Ultrahigh Vacuum. Recent Advances in Refractory Alloys for Space Power Systems. NASA SP-245, 1970, pp. 75-125.

8. Wang, Chi-Teh: Applied Elasticity. McGraw-Hill Book Co., Inc., 1953.

TABLE I. - AXIAL DYNAMIC TESTS OF T-111 AND 17-4PH STAINLESS STEEL

Test and specimen number	Collar-button vibration suppressor		Flange thickness, mm		Shaft connections to end flanges	Strain gages used	Yield stress from ref. 7, N/cm^2	End clearance, mm	Diametral clearance, mm	Results of sine tests at 5 to 2000 Hz	Test frequency, Hz	Acceleration load, g's	Time at loads, min	Maximum load, N	Stress at failure, $N\ cm^2$	Shock factor, $Y_s\ Y_s$ (b)	Total number of cycles
	Material	Shaft diameter, mm	Top	Bottom													
[a]1	T-111	1.473	0.503 (0.076 Dish)	2.235 (Flat)	Solid, solid	None	47 570	<0.025 (0.075 Dish)	<0.025	Failed at 70.2 g's, 380 Hz	5 to 2000	35 to 70.2 (Sweep test)	6.5 (Sweep test)	194	11 380	4.16	263 200
2	T-111	1.473	0.503 (0.076 Dish)	2.235 (Flat)	Solid, solid	None	47 570	<0.025 (0.075 Dish)	<0.025	Constant-frequency test only	200	5 to 45 (Failed at 45)	10 (Each g-load)	125	7 310	6.5	960 000
3	T-111	1.473	0.503 (0.076 Dish)	2.235 (Flat)	Solid, solid	None	47 570	<0.025 (0.075 Dish)	<0.025	Constant-frequency test only	200	5 to 50 (Failed at 50)	10 (Each 2-load)	139	8 140	5.84	480 000
6	17-4PH	1.732	1.397 (Flat)	1.397 (Flat)	Solid, solid	None	86 180 (91 000 to 109 600 in test)	<0.025	<0.025	Constant-frequency test only	200	20 to 72	1 (Each g-load, then 30 min at 72 g's)	199	No failure	No failure	468 000
8	17-4PH	1.524	1.397 (Flat)	1.397 (Flat)	Solid, swaged	Two mounted 90° apart on shaft	85 180	<0.025 0 >.025 >.050 >.075	<0.025 .025 .685 .685 .685	No failure, no natural frequency	20 to 2000	1 and 10	6.5 (Sweep test)	27.5	No failure	Not applicable	5 650 000
								<0.025	<0.025	No failure, no natural frequency	200	30 to 100	1 (Each g-load)	-----	No failure	---------	--------
													5 (At 100 g's)	277	Failed at 15 170	5.7	216 000
9	17-4PH	1.486	1.397 (Flat)	1.397 (Flat)	Solid, swaged	Two mounted 90° apart on shaft	86 180	<0.025	<0.025	No failure, no natural frequency	5 to 2000	1 to 5	6.5 (Sweep test)	13.8	No failure	Not applicable	211 000
10	17-4PH	1.524	1.397 (Flat)	1.397 (Flat)	Solid, swaged	None	86 180	<0.025 0.076 to 1.012	<0.025 <0.025	Constant-frequency test only	200	20 to 100	1 (Each g-load)	277	No failure	No failure	336 000
11	17-4PH	1.016	1.397 (Flat)	1.397 (Flat)	Solid, swaged	None	86 180	<0.025	<0.025	Constant-frequency test only	200	20 to 90 (Failed at 90)	1 (Each g-load)	250	30 680	2.8	132 000
12	17-4PH	1.016	1.397 (Flat)	1.397 (Flat)	Solid, swaged	None	86 180	0.075 to 1.012	<0.025	Constant-frequency test only	200	20 to 70 (Failed at 70)	1 (Each g-load)	208	25 500	3.4	108 000

[a]Specimen survived shock tests and diametral random and sine tests at Saturn specifications.

[b]Ratio of static yield stress to apparent dynamic yield stress.

TABLE II. - AXIAL STATIC TEST OF 17-4PH STAINLESS STEEL

Test and specimen number	Shaft diameter, mm	Shaft connections to end flanges (a)	Mounting remarks	Maximum load, N	0.2 Percent offset yield stress, N/cm^2 (b)	Ultimate stress, N/cm^2	Remarks
4	1.610	Solid, solid	<0.025-mm side clearance	2220	103 400	109 600	Abnormally large amount of strain was recorded when testing maching strip recorder was used; this strain included specimen, fixture, and tensil tester; accurate yield point was not possible
5	1.514	Solid, solid	No side support	1445	80 300	80 300	Specimen had no lateral support and top face moved laterally when shaft yielded
7	1.727	Solid, swaged	<0.025-mm side clearance	2450	91 300	104 800	Same as remarks for test 4
9	1.486	Solid, swaged	<0.025-mm side clearance	1670	95 800	95 800	Only specimen strains were recorded when two strain gages were used (gages mounted 90° apart on specimen shaft)

[a]Top and bottom flange thickness, 1.397 mm; some specimens were machined as one piece, for others a shaft and flange were machined and a separate bottom flange was swaged to the shaft.

[b]Yield stress from ref. 6, 86 000 N/cm^2; specimens heat treated 4 hr at 894 K (1150° F).

TABLE III. - AXIAL DYNAMIC TESTS OF INGOT IRON SUPPRESSORS

[All flanges were flat and 1.396 mm thick; flanges and shafts were one piece; tested yield stress, 19 410 N/cm^2; diametral clearances, <0.025 mm; only sine tests at 200 Hz; all loads held for 1 min.]

Test and specimen number	Shaft diameter, mm	End clearance, mm	Acceleration load, g's	Maximum loading, N	Stress at failure, Y_d, newton/cm^2	Shock factor, Y_s/Y_d (a)	Total number of cycles
1	1.524	<0.025	5, 10, 15 20, 25, 30 35, 40	110.6	6060	3.2	16 000
2	1.511	0.075 to 0.100	5, 10, 15 17, 19, 21 23	58.3	3180	6.1	11 000
3	1.524	0.038 to 0.064	5, 10, 15 20, 22, 24 26, 28, 30	82.7	4560	4.26	17 000
4	1.534	<0.025	5, 10, 15 20, 25, 30 35, 37, 39	107.8	5840	3.3	19 000
5	1.524	0.075 to 0.100	5, 10, 15 17, 19, 21 22, 23	62.7	3490	5.5	14 000

[a]Ratio of static yield stress to apparent dynamic yield stress.

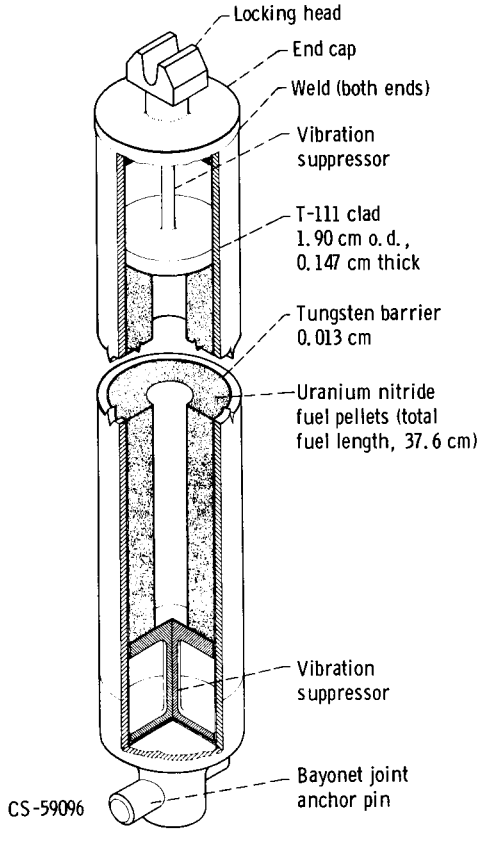

Figure 1. - Typical fuel-element cross section.

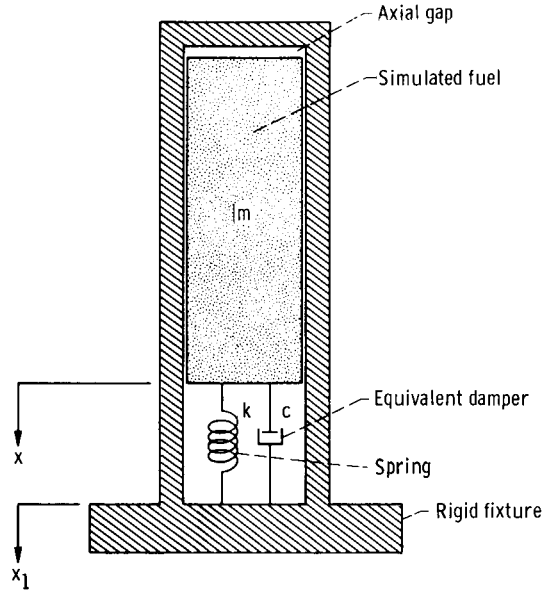

Figure 2. - Fuel-pin model.

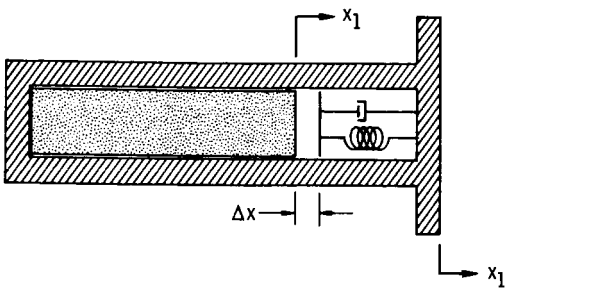

(a) Fuel velocity same as fixture; fuel accelerates to v_{max}.

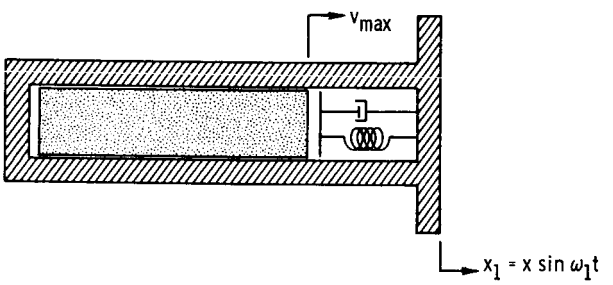

(b) Fuel mass velocity is greater than that of fixture; fuel is at constant velocity.

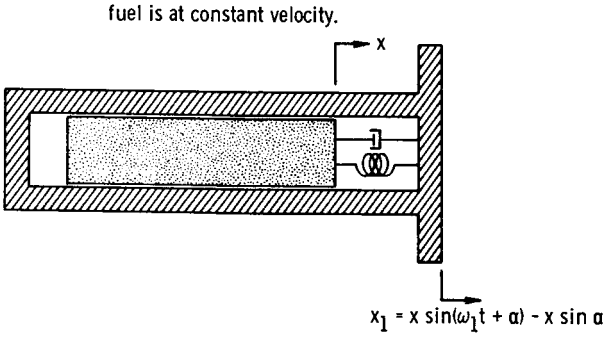

(c) Impact and spring compression.

Figure 3. - Sequence of events leading to impact and spring compression.

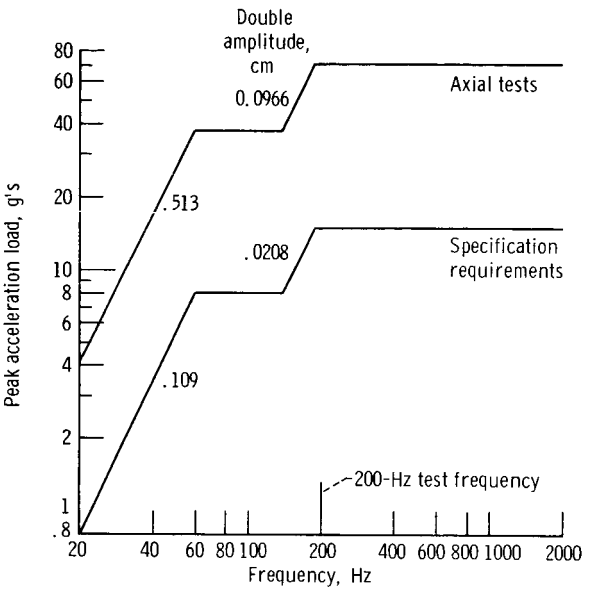

Figure 4. - Peak acceleration loading as function of frequency for sinusoidal vibration tests.

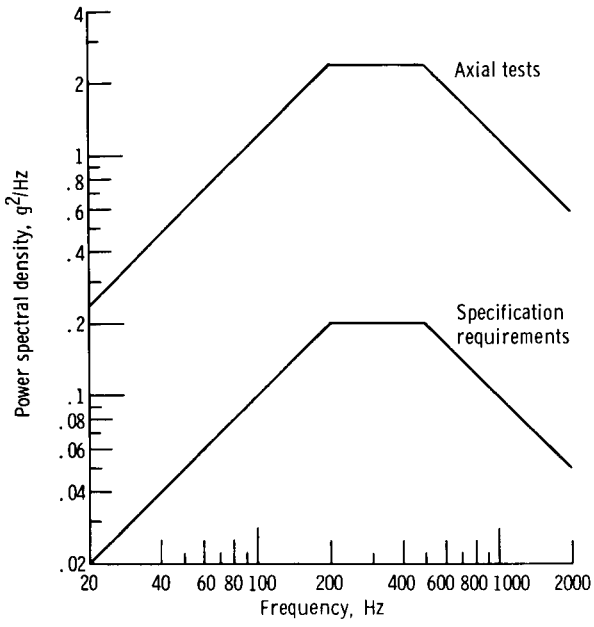

Figure 5. - Power spectral density as function of frequency for random vibration tests. Curve slope, 3 decibels per octave.

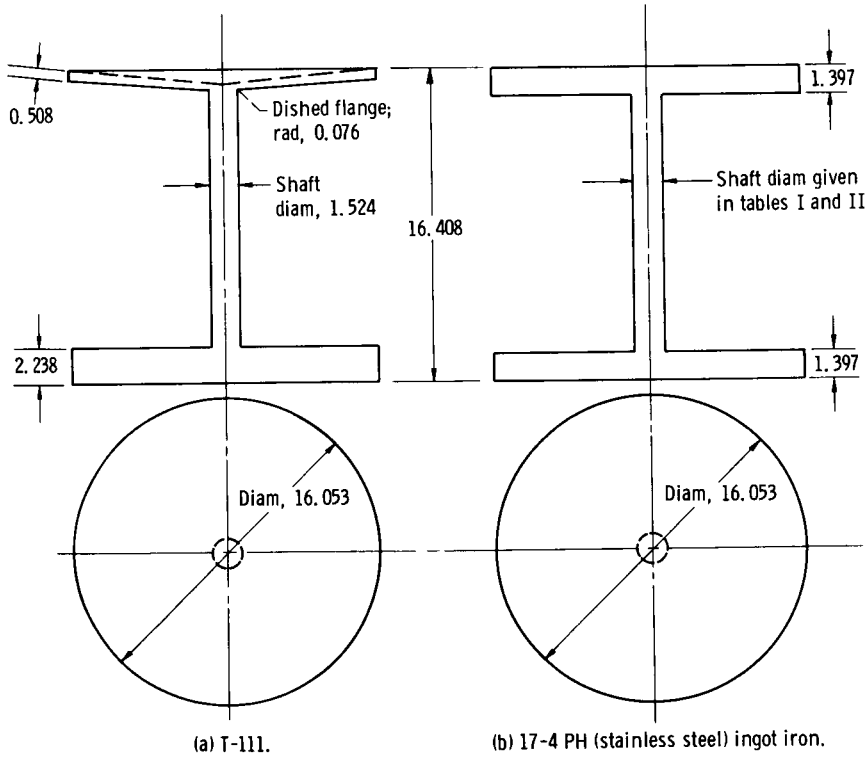

(a) T-111.

(b) 17-4 PH (stainless steel) ingot iron.

Figure 6. - Geometry and material of vibration suppressors. (Dimensions in millimeters.)

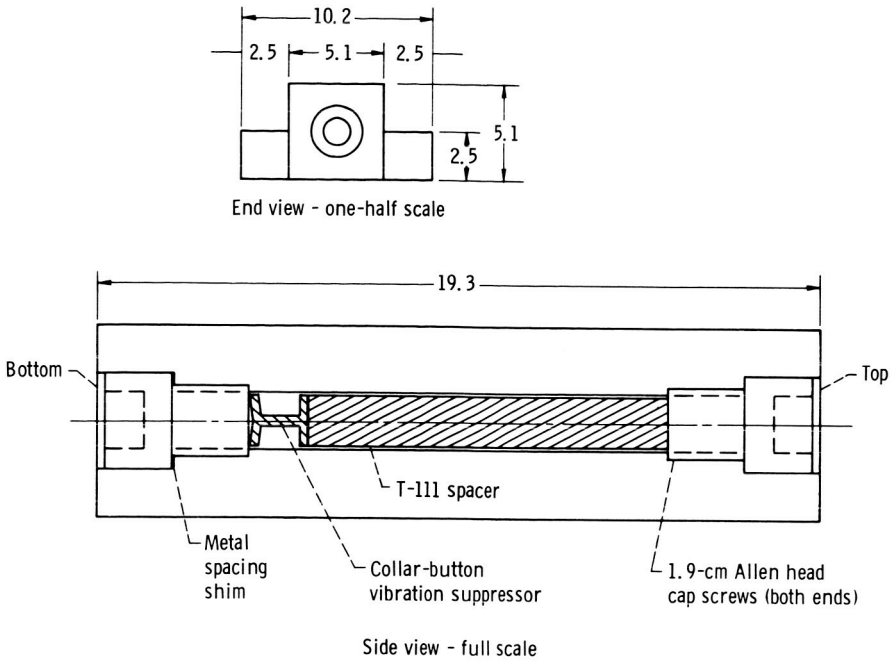

Figure 7. - Complete test fixture with collar-button vibration suppressor. (Dimensions in centimeters.)

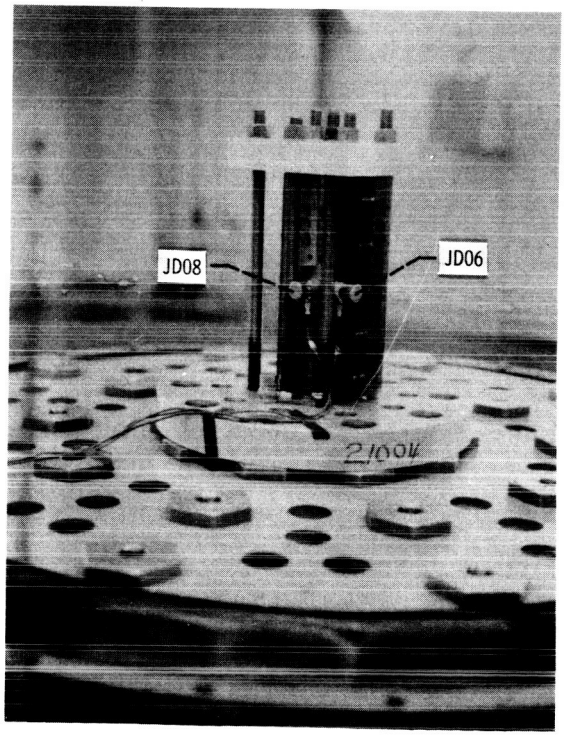

Figure 8. - Fixture with accelerometers mounted in vertical position on shaker table.

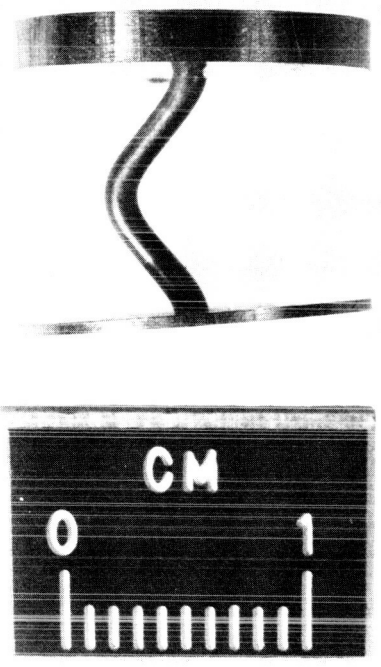

C-70-708

Figure 9. - T-111 vibration suppressor after failing during vibration test.

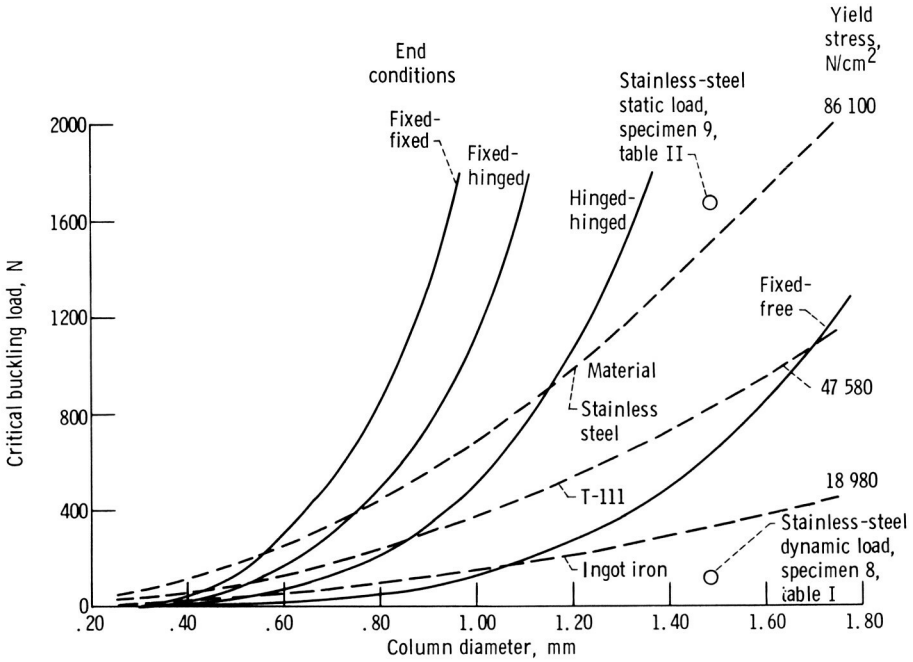

Figure 10. - Critical buckling and yield loads for various column diameters. Critical load = $c\pi EI/l^2$, where c is the coefficient of damping, E is the modulus of elasticity (19 650 N/cm^2), I is the moment of inertia of the column, and l is the column length (1.362 cm) (ref. 8).

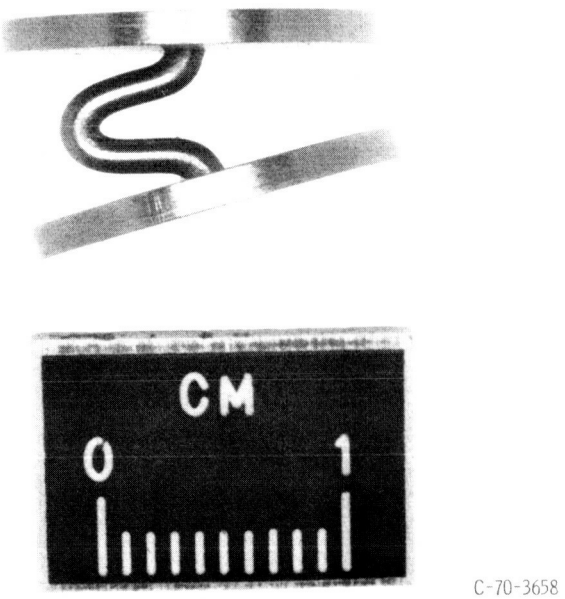

Figure 11. - Ingot iron vibration suppressor after failing at 40 g and 200 hertz.

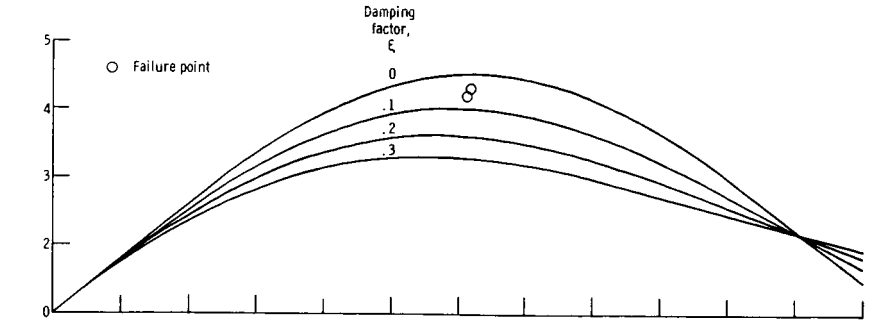

(a) Axial gap, 0.025 millimeter; acceleration loading, 40 g's.

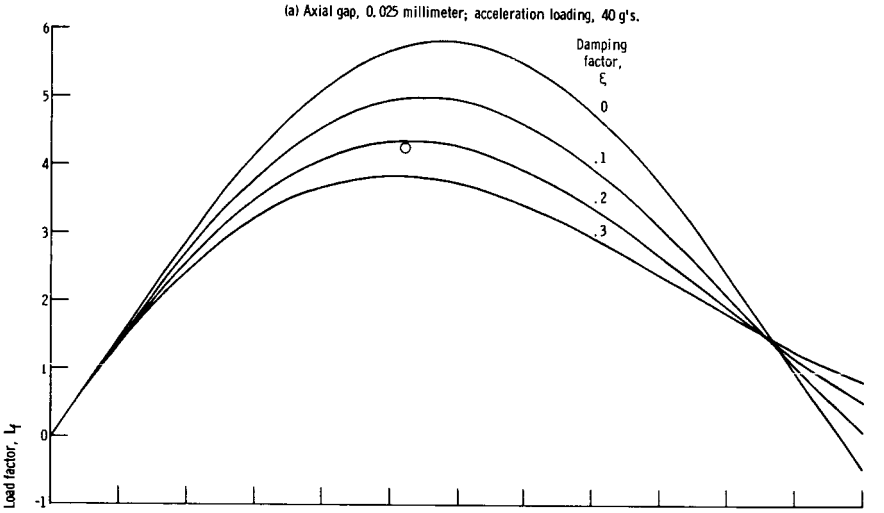

(b) Axial gap, 0.050 millimeter; acceleration loading, 30 g's.

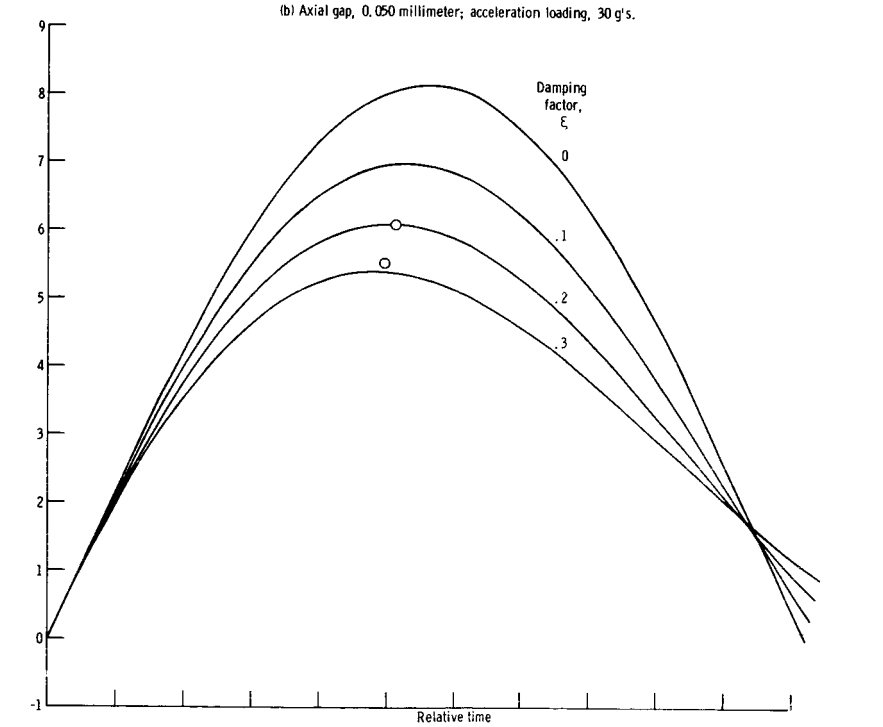

(c) Axial gap, 0.076 millimeter; acceleration loading, 23 g's.

Figure 12. - Load factor for vibration suppressor at test conditions.

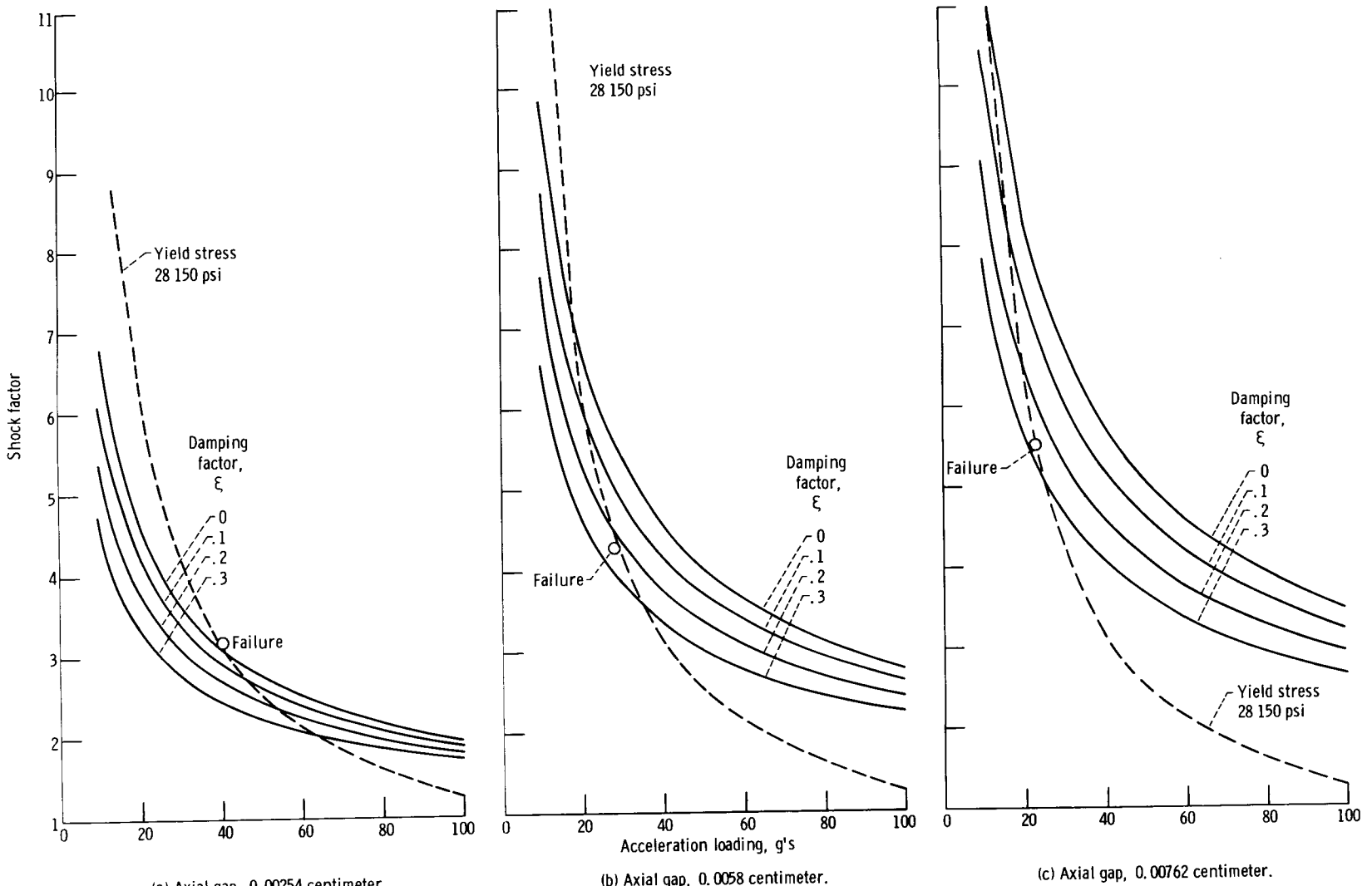

Figure 13. - Shock factor as function of acceleration loading. Column diameter, 0.152 centimeter; modulus of elasticity, 17.9×10^6 Newtons per square centimeter; column length, 1.37 centimeters; frequency, 200 hertz; mass, 0.284 kilogram.

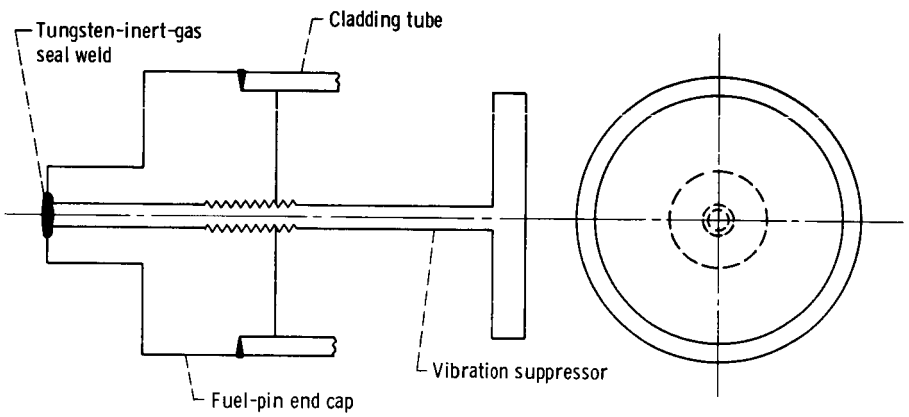

Figure 14. - Fuel-pin end cap with modified vibration suppressor.